Nuclear Science and Techniques (2024) 35:139
https://doi.org/10.1007/s41365-024-01532-z

Robustness of the octupole collectivity in ^{144}Ba within the cranking covariant density functional theory in 3D lattice

Ze-Kai Li[1] · Yuan-Yuan Wang[1,2]

Received: 19 March 2024 / Revised: 30 May 2024 / Accepted: 5 June 2024 / Published online: 7 August 2024

Abstract
The octupole deformation and collectivity in octupole double-magic nucleus ^{144}Ba are investigated using the Cranking covariant density functional theory in a three-dimensional lattice space. The reduced $B(E3)$ transition probability is implemented for the first time in semiclassical approximation based on the microscopically calculated electric octupole moments. The available data, including the I-ω relation and electric transitional probabilities $B(E2)$ and $B(E3)$ are well reproduced. Furthermore, it is shown that the ground state of ^{144}Ba exhibits axial octupole and quadrupole deformations that persist up to high spins ($I \approx 24\hbar$).

Keywords Octupole collectivity · Cranking covariant density functional theory · Rotational spectrum · Electric transitional probabilities

1 Introduction

As a microscopic quantum many-body system, the atomic nucleus carries a wealth of symmetries and symmetry breakings. Spontaneous symmetry breaking plays a crucial role in understanding the structure of atomic nuclei. Reflection symmetry breaking of atomic nuclei occurs in nuclei with octupole deformations (such as pear-shaped nuclei) [1–3]. This is related to the charge parity (CP) symmetry violation beyond the standard model [4] and has been at the frontier of both nuclear physics and particle physics.

The study of reflection symmetry breaking in pear-shaped nuclei can be traced back to the 1950 s and is characterized by the occurrence of interleaved positive- and negative-parity bands in even-even nuclei, parity doublet bands in odd-mass nuclei, and enhanced electric dipole ($E1$) and octupole ($E3$) moments [1–3]. The pear shapes of the nucleus can arise from the strong octupole correlations of the nucleons near the Fermi surface. They occupy states of opposite parity with the orbital and total angular momenta differing by $3\hbar$, i.e., $\Delta l = \Delta j = 3\hbar$. Empirically, this condition occurs for a proton or neutron particle numbers: 34 ($g_{9/2} \leftrightarrow p_{3/2}$), 56 ($h_{11/2} \leftrightarrow d_{5/2}$), 88 ($i_{13/2} \leftrightarrow f_{7/2}$), and 134 ($j_{15/2} \leftrightarrow g_{9/2}$)[1]. To date, the octupole correlations and pear-shaped nuclei have been extensively studied in the A ∼80 mass region with $Z \approx 34$ [5, 6], in the A ∼150 mass region with $Z \approx 56$ and $N \approx 88$ [7–9], and in the A ∼220 mass region, with $Z \approx 88$ and $N \approx 134$, see the reviews [1–3].

Focusing on barium isotopes in A ∼150 mass region, the nucleus ^{144}Ba is of continuous interest due to its octupole double-magic character with proton and neutron numbers $Z = 56$ and $N = 88$, respectively. Experimentally, various signatures including the low-lying negative-parity states, the interleaved positive- and negative-parity bands with enhanced $E1$ connecting transitions [10–13], and especially the enhanced $E3$ transition strengths [14], represent an unambiguous static nuclear octupole deformation in ^{144}Ba. Theoretically, the octupole deformation and collectivity in ^{144}Ba have been studied by using various approaches, such as cranked Woods-Saxon-Bogoliubov theory [15], self-consistent cranked Hartree-Fock-Bogoliubov (HFB) calculation with parity projection [16], a

This work was partly supported by the National Natural Science Foundation of China (NSFC) (No. 12205097) and the Fundamental Research Funds for the Central Universities (No. 2024MS071).

✉ Yuan-Yuan Wang
yywang1021@ncepu.edu.cn

[1] Mathematics and Physics Department, North China Electric Power University, Beijing 102206, China

[2] Hebei Key Laboratory of Physics and Energy Technology, North China Electric Power University, Baoding 071000, China

one-dimensional collective model with phenomenological spin-dependent potentials [17–19], the quadrupole-octupole collective model [20, 21], cluster model [22, 23], potential energy surface calculations [24], the reflection-asymmetric relativistic mean field (RAS-RMF) approach [25–28], the interacting boson model (IBM) [29, 30], the generator coordinate method (GCM) based on nonrelativistic [31], and relativistic density functional theories [32, 33].

The nuclear density functional theory (DFT) starts with a universal energy density functional and can achieve a self- consistent description for almost all nuclei [34, 35]. Over the past decades, relativistic or covariant version of DFT (CDFT) have been developed and widely applied to investigate a large variety of nuclear phenomena [36–46]. To describe the nuclear spectroscopic properties, cranking CDFT has been developed and widely applied to investigate both the ground states of nuclei and various rotational excitation phenomena [47–50]. Specifically, cranking CDFT in a three-dimensional (3D) lattice space was realized in Ref. [51] and has been widely applied to investigate the exotic shapes of nuclei and their excitation modes such as the nuclear linear chain [51, 52], toroidal structures [53], and nuclear chiral rotation [54]. It provides a useful way to understand the current focus of the observed rotational bands in octupole double-magic nucleus ^{144}Ba, since in 3D lattice calculations, the single-particle wave functions have no symmetry limitation in space and all deformation degrees of freedom of the nucleus are self-consistent included.

In this study, the cranking CDFT in 3D lattice space is used to investigate the octupole deformation and collectivity in the nucleus ^{144}Ba. The model is shown briefly in Sect. 2. The numerical details and calculated results for the available data, including the I–ω relation and electromagnetic transition probabilities, are shown in Sect. 3. A summary is shown in Sect. 4.

2 Theoretical Framework

The detailed formalism of the cranking CDFT in 3D lattice space has been shown in Ref. [51]. The starting point of the CDFT is a standard effective nuclear Lagrangian density, where the nucleons are coupled with a meson exchange interaction [55–57] or zero-range point-coupling interaction [58–60] as follows,

$$
\begin{aligned}
\mathcal{L} &= \mathcal{L}^{\rm free} + \mathcal{L}^{\rm 4f} + \mathcal{L}^{\rm hot} + \mathcal{L}^{\rm der} + \mathcal{L}^{\rm em} \\
&= \bar\psi(i\gamma_\mu\partial^\mu - m)\psi - \frac{1}{2}\alpha_{\rm S}(\bar\psi\psi)(\bar\psi\psi) - \frac{1}{2}\alpha_{\rm V}(\bar\psi\gamma_\mu\psi)(\bar\psi\gamma^\mu\psi) \\
&- \frac{1}{2}\alpha_{\rm TS}(\bar\psi\tau\psi)(\bar\psi\tau\psi) - \frac{1}{2}\alpha_{\rm TV}(\bar\psi\tau\gamma_\mu\psi)(\bar\psi\tau\gamma^\mu\psi) \\
&- \frac{1}{3}\beta_{\rm S}(\bar\psi\psi)^3 - \frac{1}{4}\gamma_{\rm S}(\bar\psi\psi)^4 - \frac{1}{4}\gamma_{\rm V}[(\bar\psi\gamma_\mu\psi)(\bar\psi\gamma^\mu\psi)]^2 \\
&- \frac{1}{2}\delta_{\rm S}\partial_\nu(\bar\psi\psi)\partial^\nu(\bar\psi\psi) - \frac{1}{2}\delta_{\rm V}\partial_\nu(\bar\psi\gamma_\mu\psi)\partial^\nu(\bar\psi\gamma^\mu\psi) \\
&- \frac{1}{2}\delta_{\rm TS}\partial_\nu(\bar\psi\tau\psi)\partial^\nu(\bar\psi\tau\psi) - \frac{1}{2}\delta_{\rm TV}\partial_\nu(\bar\psi\tau\gamma_\mu\psi)\partial^\nu(\bar\psi\tau\gamma_\mu\psi) \\
&- \frac{1}{4}F^{\mu\nu}F_{\mu\nu} - e\frac{1-\tau_3}{2}\bar\psi\gamma^\mu\psi A_\mu.
\end{aligned} \tag{1}
$$

In Eq. (1), m denotes the nucleon mass, e denotes the charge unit of the protons, A_μ and $F_{\mu\nu}$ denote the four-vector potential and field strength tensor of the electromagnetic field, respectively. For the 11 coupling constants, α_S, $\alpha_{\rm V}$, $\alpha_{\rm TS}$, $\alpha_{\rm TV}$, $\beta_{\rm S}$, $\gamma_{\rm S}$, $\gamma_{\rm V}$, $\delta_{\rm S}$, $\delta_{\rm V}$, $\delta_{\rm TS}$, and $\delta_{\rm TV}$, α refers to the four-fermion term, β and γ refer to the third- and fourth-order terms, respectively, and δ refers to the derivative couplings. Subscripts S, V, and T indicate the symmetries of the couplings, i.e., S denotes a scalar, V denotes a vector, and T denotes an isovector.

To describe nuclear rotations in the cranking approximation, the effective Lagrangian density of Eq. (1) is transformed into a rotating frame with a constant rotational frequency ω around the rotational axis. The equation of the single-particle motion can be derived from the Lagrangian in the rotating frame:

$$
\hat h'\psi_k = (\hat h_0 - \boldsymbol\omega\cdot\hat{\mathbf J})\psi_k = \varepsilon'_k\psi_k, \tag{2}
$$

with $\hat h'$ denoting the cranking single-particle Hamiltonian, $-\boldsymbol\omega\cdot\hat{\mathbf J}$ denoting the Coriolis or cranking term, ε'_k denoting the single-particle Routhians, and $\hat{\mathbf J} = \hat{\mathbf l} + \frac{1}{2}\hat{\boldsymbol\Sigma}$ denoting the total angular momentum of the nucleon spinors. The single-particle Hamiltonian $\hat h_0$ is

$$
\hat h_0 = \boldsymbol\alpha\cdot[-{\rm i}\boldsymbol\nabla - \mathbf V(\mathbf r)] + \beta[m_N + S(\mathbf r)] + V_0(\mathbf r). \tag{3}
$$

The relativistic scalar $S(\mathbf r)$ and vector field $V_\mu(\mathbf r)$ are connected in a self-consistent manner to the nucleon density and current distribution. By solving the cranking Dirac equation (2) self-consistently at a given rotational frequency, the single-particle Routhians, expectation values of the angular momentum, and quadrupole and octupole moments can be obtained, see Refs. [34, 61–63] for the detailed formalism. Specifically, single-particle wave functions have no symmetry limitation in space and all nuclear deformation degrees of freedom including octupole deformation are self-consistently obtained in the present 3D lattice cranking CDFT calculation. It provides a powerful way to investigate the evolution of octupole shapes with spin in the current octupole double-magic nucleus ^{144}Ba.

The quadrupole moments ($Q_{20}, Q_{2\pm1}, Q_{2\pm2}$) and octupole moments ($Q_{30}, Q_{3\pm1}, Q_{3\pm2}, Q_{3\pm3}$) can be calculated as:

$$Q_{20} = \sqrt{\frac{5}{16\pi}}\langle 3z^2 - r^2\rangle, \tag{4}$$

$$Q_{21} = -Q^*_{2-1} = -\sqrt{\frac{15}{32\pi}}\langle (x+iy)z\rangle, \tag{5}$$

$$Q_{22} = Q_{2-2} = \sqrt{\frac{15}{32\pi}}\langle x^2 - y^2\rangle, \tag{6}$$

$$Q_{30} = \sqrt{\frac{7}{16\pi}}\langle (2z^2 - 3x^2 - 3y^2)z\rangle, \tag{7}$$

$$Q_{31} = -Q^*_{3-1} = -\sqrt{\frac{21}{64\pi}}\Big[\langle (4z^2 - x^2 - y^2)x\rangle + \mathrm{i}\langle (4z^2 - x^2 - y^2)y\rangle\Big], \tag{8}$$

$$Q_{32} = Q^*_{3-2} = \sqrt{\frac{105}{32\pi}}\Big[\langle (x^2 - y^2)z\rangle + \mathrm{i}\langle xyz\rangle\Big], \tag{9}$$

$$Q_{33} = -Q^*_{3-3} = -\sqrt{\frac{35}{64\pi}}\Big[\langle (x^2 - 3y^2)x\rangle + \mathrm{i}\langle (3x^2 - y^2)y\rangle\Big]. \tag{10}$$

Since, the nuclei are placed in a 3D lattice space, we additionally constrain the center of mass of the entire nucleus at the origin and align the principal axes with the coordinate axes to remove redundant degrees of freedom. The values of Q_{21} and Q_{2-1} always disappear. The deformation parameters $\beta_{\lambda\mu}$ can be obtained from the corresponding multipole moments [64]

$$\beta_{\lambda\mu} = \frac{4\pi}{3NR^\lambda}Q_{\lambda\mu} \tag{11}$$

with $R = 1.2A^{1/3}$ fm and N denoting the number of protons neutrons, or nucleons.

Based on the quadrupole moments, $B(E2)$ transition probabilities can be derived in semiclassical approximation [50, 65]

$$B(E2) = \frac{3}{8}\left[Q^{\mathrm{p}}_{20}\sin^2\theta + \sqrt{\frac{2}{3}}Q^{\mathrm{p}}_{22}\cos 2\varphi\right]^2 + (Q^{\mathrm{p}}_{22}\cos\theta\sin 2\varphi)^2, \tag{12}$$

where Q^{p}_{20} and Q^{p}_{22} denote the quadrupole moments of the protons, and θ , and φ denote the polar and azimuthal angles of the total angular momentum in the intrinsic frame, respectively. Similarly, $B(E3)$ transition probabilities can be derived in semiclassical approximation:

$$\begin{aligned} B(E3) = \Bigg[& \frac{\sqrt{5}}{4}\sin^3\theta Q^{\mathrm{p}}_{30} \\ & + \frac{\sqrt{15}}{4}\sin^2\theta\cos\theta\Big(\cos\varphi\,\mathrm{Re}[Q^{\mathrm{p}}_{31}] + \sin\varphi\mathrm{Im}[Q^{\mathrm{p}}_{31}]\Big) \\ & + \frac{\sqrt{6}}{4}\sin\theta(1+\cos^2\theta)\Big(\cos 2\varphi\mathrm{Re}[Q^{\mathrm{p}}_{32}] + \sin 2\varphi\mathrm{Im}[Q^{\mathrm{p}}_{32}]\Big) \\ & + \frac{1}{4}(3+\cos^2\theta)\cos\theta\Big(\cos 3\varphi\mathrm{Re}[Q^{\mathrm{p}}_{33}] + \sin 3\varphi\mathrm{Im}[Q^{\mathrm{p}}_{33}]\Big)\Bigg]^2 \\ + \Bigg[& \frac{\sqrt{15}}{4}\sin^2\theta\Big(\cos\varphi\,\mathrm{Im}[Q^{\mathrm{p}}_{31}] - \sin\varphi\mathrm{Re}[Q^{\mathrm{p}}_{31}]\Big) \\ & + \frac{\sqrt{6}}{2}\sin\theta\cos\theta\Big(\cos 2\varphi\mathrm{Im}[Q^{\mathrm{p}}_{32}] - \sin 2\varphi\mathrm{Re}[Q^{\mathrm{p}}_{32}]\Big) \\ & + \frac{1}{4}(1+3\cos^2\theta)\Big(\cos 3\varphi\mathrm{Im}[Q^{\mathrm{p}}_{33}] - \sin 3\varphi\mathrm{Re}[Q^{\mathrm{p}}_{33}]\Big)\Bigg]^2, \end{aligned} \tag{13}$$

where Q^{p}_{30}, $Q^{\mathrm{p}}_{3\pm1}$, $Q^{\mathrm{p}}_{3\pm2}$, and $Q^{\mathrm{p}}_{3\pm3}$ are the octupole moments of protons.

3 Results and Discussion

A successful density functional PC-PK1 [60] is employed in the CDFT calculation. The Dirac spinors of the nucleons and potentials in the single-particle Hamiltonian (2) are represented in 3D lattice space. The step size and grid number along x, y, and z axes are chosen as 1 fm and 30, respectively. The convergence of the iteration is realized by ensuring that the energy uncertainty for every occupied single-particle state is smaller than 10^{-9} MeV^2 and the maximum absolute difference between the mean potentials at two adjacent iterations is smaller than 10^{-3} MeV. To provide the potential energy surface in the (β_{20}, β_{30}) plane, a deformation-constrained CDFT calculation in 3D lattice space is performed in the region $\beta_{20} \in [-0.3, 0.4]$ and $\beta_{30} \in [0.0, 0.3]$ with a step size of 0.05. For cranking CDFT calculations, the rotational frequency is varied from $\omega = 0.0$ to 0.45 MeV.

In Fig. 1, the potential energy surface (PES) in the (β_{20}, β_{30}) plane for ^{144}Ba calculated by the constrained CDFT calculation in a 3D lattice with the successful density functional PC-PK1 is shown [60]. It shows that the global minimum of the PES locates at $\beta_{20} = 0.22$ and $\beta_{30} = 0.13$. It should be noted that the single-particle wave functions calculated in the present CDFT calculation have no symmetry limitation, and all deformation degrees of freedom of the nucleus are self-consistent included. Apart from the constrained axially symmetric quadrupole and octupole deformations β_{20} and β_{30}, the axially symmetric hexadecapole deformation $\beta_{40} = 0.13$ is also obtained self-consistently for the ground state of ^{144}Ba. All axial asymmetric deformations, i.e., $\beta_{2\mu}, \beta_{3\mu}, \beta_{4\mu}, (\mu \neq 0)$, are found to be zero, which implies that the ground state of ^{144}Ba corresponds to an axially symmetric and reflection-asymmetric

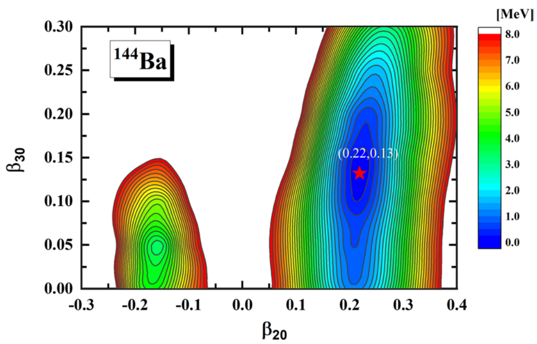

Fig. 1 Potential energy surface for ^{144}Ba calculated by the CDFT in 3D lattice [51] with density functional PC-PK1 [60]. The contour separation is 0.25 MeV and the pentagram corresponds to the location of the ground state

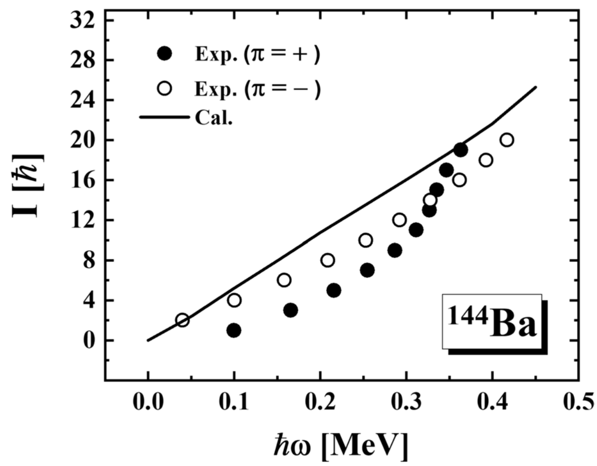

Fig. 2 Total angular momentum as a function of the rotational frequency for the ground state band of ^{144}Ba calculated by the cranking CDFT in 3D lattice (line) in comparison with the experimental interleaved positive-parity (solid symbols) and negative-parity bands (open symbols)

shape. Around the minimum, the PES exhibits a relatively soft character. The energy difference between the ground state ($\beta_{20} = 0.22$, $\beta_{30} = 0.13$) and the lowest reflection symmetric energy position ($\beta_{20} = 0.2$, $\beta_{30} = 0.0$) is less than 1.0 MeV. Moreover, a secondary minimum (~3.0 MeV) is observed at ($\beta_{20} = -0.15$, $\beta_{30} = 0.05$). Experimentally, a value of $\beta_{30} = 0.17(^{+4}_{-6})$ has been derived [14] by using the relationship of the octupole moment (with the standard assumption of axial symmetry) and the commonly used β_{30} parameters [66]. The obtained ground state octupole deformation $\beta_{30} = 0.13$ is consistent with the β_{30} value within the experimental error range. As analyzed in Ref. [25], this octupole deformation minimum is a consequence of strong octupole–octupole interactions between pairs of single-particle orbitals near the Fermi surface with $\Delta l = \Delta j = 3\hbar$ around the Fermi level, i.e., proton ($h_{11/2} \leftrightarrow d_{5/2}$) and neutron ($i_{13/2} \leftrightarrow f_{7/2}$).

To investigate the observed rotational spectroscopic properties and the evolution of the octupole deformation and collectivity with respect to nuclear rotation, cranking CDFT calculations in 3D lattice are performed. Figure 2 shows the calculated total angular momentum as a function of the rotational frequency for the ground state band in ^{144}Ba comparison with the available data [13]. It can be seen that the experimental data are slightly overestimated by the present calculated results, which give an excessive moment of inertia. A better agreement with the experimental data is expected by taking into account the pairing correlation [67] for which the moments of inertia will be depressed.

With the quadrupole and octupole moments obtained self-consistently, the reduced transition probabilities $B(E2)$ and $B(E3)$ can be calculated in semiclassical approximation according to Eqs. (12) and (13). In Fig. 3 (a), the calculated $B(E2)$ values are compared with available data [14]. It is found that the resulting $B(E2)$ values are in good agreement with the data on the order of magnitude. As shown in Fig. 3 (a), the calculated $B(E2)$ values remain nearly constant with increasing rotational frequency, which can be further understood by the changes in the quadrupole deformation shown in Fig. 4 (a). With the increasing rotational frequency, the nucleus undergoes a nearly unchanged β_{20} deformation from 0.22 to 0.20.

The octupole collectivity is also demonstrated by $B(E3)$ values shown in Fig. 3(b) and the evolution of octupole deformation β_{30} in Fig. 4(b). As shown in Fig. 3(b), the

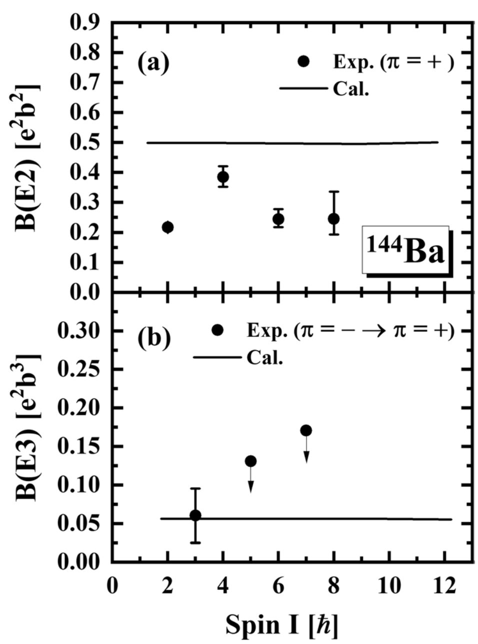

Fig. 3 Calculated (a) $B(E2)$ and (b) $B(E3)$ values as functions of the total angular momentum in the cranking CDFT calculations compared with the data for ^{144}Ba [14]

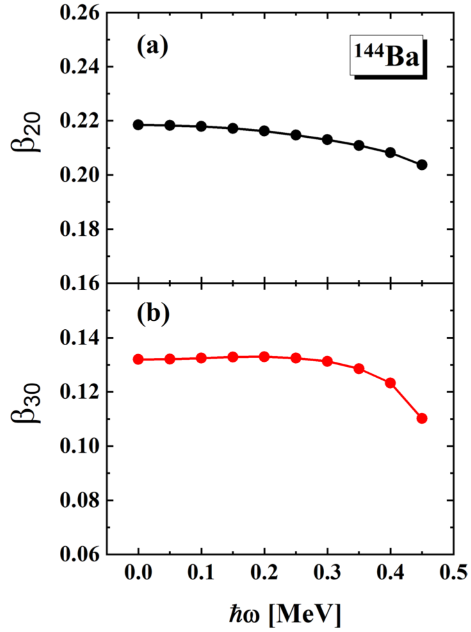

Fig. 4 Evolution of (a) quadrupole deformation β_{20} and (b) octupole deformation β_{30} for the calculated yrast states in ^{144}Ba as functions of the rotational frequency

corresponding $B(E3)$ data are effectively reproduced by the cranking CDFT calculation. As shown in Fig. 4(b), the calculated octupole deformation β_{30} increases slightly and then decreases with increasing spin. With an increase in the rotational frequency to $\hbar\omega = 0.45$ MeV (spin $I \approx 24\hbar$), the average octupole deformation is approximately $\beta_{30} = 0.128$, indicating the robustness of the octupole shape with respect to nuclear rotation.

To understand the evolution of the octupole deformation of the yrast states in ^{144}Ba, the single-proton and single-neutron Routhians are shown as functions of rotational frequency in Figs. 5 (a) and 5 (b), respectively. The levels near the Fermi surface are labeled by Nilsson-like notation $\Omega[Nn_z m_l]$ of the largest component. It is noted that these levels can mix different components with opposite parity due to the existence of octupole deformations. As shown in Fig. 5 (a) for single-proton Routhians, an energy gap $Z = 56$ fenced with several levels near the Fermi surface, is found at the ground state and persistently presented with an increase in the rotational frequency. Furthermore, an energy gap $N = 88$ for the single-neutron Routhians shown in Fig. 5(b) is found not only in the ground state, but also in the high-spin region. Therefore, it is concluded that these two energy gaps, $Z = 56$ and $N = 88$, near the Fermi surfaces are responsible for the octupole minimum and robustness of the octupole shape against nuclear rotations in ^{144}Ba.

4 Summary

In summary, the cranking covariant density functional theory in a three-dimensional lattice is first applied to investigate the octupole deformation and collectivity in octupole double-magic nucleus ^{144}Ba. With the electric octupole moments obtained by self-consistently solving the cranking Dirac equation, the reduced transition probabilities $B(E3)$ are derived in semiclassical approximation for the first time. The available data, including the $I - \omega$ relation, the $B(E2)$ and $B(E3)$ values, are well reproduced by the cranking CDFT calculations. The potential energy surface (PES) in (β_{20}, β_{30}) plane, calculated by the constrained CDFT calculation in 3D lattice, provide a static axial octupole and quadruple deformed ground state for ^{144}Ba. With the increase of the rotational frequency (up to $\hbar\omega = 0.45$ MeV), the calculated octupole deformation is nearly unchanged and give an average value $\beta_{30} = 0.128$, indicating the robustness of the octupole shape against nuclear rotation. By analyzing the single-proton and single-neutron Routhians with the increasing rotational frequency, two energy gaps, $Z = 56$ and $N = 88$, near the Fermi surfaces are found to be responsible for the octupole minimum and the robustness of the octupole shape against nuclear rotation in ^{144}Ba.

It should be noted that the pairing correlations were neglected in the present calculations. It would be interesting to introduce, for example, the shell-model-like approach [65, 67] to the present cranking CDFT in 3D lattice to investigate the effects of pairing correlations. The current cranking CDFT describes the physics only on average in a rotating

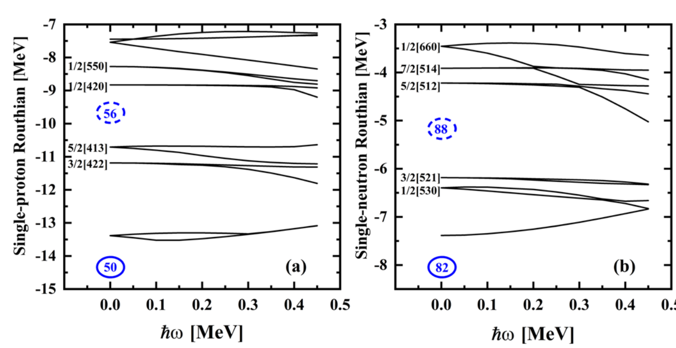

Fig. 5 Single-particle Routhians for (a) proton and (b) neutron of ^{144}Ba as functions of the rotational frequency. The levels near the Fermi surface are labeled by Nilsson-like notations $\Omega[Nn_z m_l]$ of the largest component

mean field. The total angular moment is treated in semi-classical approximation and the total parity is not a good quantum number. For the interleaved positive- and negative-parity bands in octupole deformed nuclei, the total parity and parity splitting cannot be calculated using the present 3D lattice cranking CDFT calculation. Additionally, it will be interesting to introduce the parity projection beyond 3D lattice cranking CDFT in the future.

Acknowledgements We are gratefully for the fruitful discussions with Prof. Peng-Wei Zhao, Prof. Shuang-Quan Zhang, Dr. Zheng-Xue Ren, Dr. Xin-Hui Wu, Dr. Ya-Kun Wang, Bo Li, and Fang-Fang Xu.

Author contributions All authors contributed to the study conception and design. Material preparation, data collection and analysis were performed by Yuan-Yuan Wang and Ze-Kai Li. The first draft of the manuscript was written by Yuan-Yuan Wang and all authors commented on previous versions of the manuscript. All authors read and approved the final manuscript.

Data availibility The data that support the findings of this study are openly available in Science Data Bank at https://cstr.cn/31253.11.sciencedb.j00186.00114 and https://www.doi.org/10.57760/sciencedb.j00186.00114.

Declarations

Conflict of interest The authors declare that they have no Conflict of interest.

References

1. P.A. Butler, W. Nazarewicz, Intrinsic reflection asymmetry in atomic nuclei. Rev. Mod. Phys. **68**, 349 (1996). https://doi.org/10.1103/RevModPhys.68.349
2. P.A. Butler, Octupole collectivity in nuclei. J. Phys. G Nucl. Part. Phys. **43**, 073002 (2016). https://doi.org/10.1098/rspa.2020.0202
3. P.A. Butler, Pear-shaped atomic nuclei. Proc. R. Soc. A **476**, 20200202 (2020). https://doi.org/10.1088/0954-3899/43/7/073002
4. L.P. Gaffney, P.A. Butler, M. Scheck et al., Studies of pear-shaped nuclei using accelerated radioactive beams. Nature **497**, 199 (2013). https://doi.org/10.1038/nature12073
5. C. Liu, S.Y. Wang, R.A. Bark et al., Evidence for octupole correlations in multiple chiral doublet bands. Phys. Rev. Lett. **116**, 112501 (2016). https://doi.org/10.1103/PhysRevLett.116.112501
6. S. Bhattacharya, T. Trivedi, D. Negi et al., Evolution of collectivity and evidence of octupole correlations in ^{73}Br. Phys. Rev. C **100**, 014315 (2019). https://doi.org/10.1103/PhysRevC.100.014315
7. S.J. Zhu, J.H. Hamilton, A.V. Ramayya et al., Octupole correlations in neutron-rich ^{143,145}Ba and a type of superdeformed band in ^{145}Ba. Phys. Rev. C **60**, 051304 (1999). https://doi.org/10.1103/PhysRevC.60.051304
8. X.C. Chen, J. Zhao, C. Xu et al., Evolution of octupole correlations in ^{123}Ba. Phys. Rev. C **94**, 021301 (2016). https://doi.org/10.1103/PhysRevC.94.021301
9. B.F. Lv, C.M. Petrache, K.K. Zheng et al., Refined description of the positive-parity bands and the extent of octupole correlations in ^{120}Ba. Phys. Rev. C **105**, 044319 (2016). https://doi.org/10.1103/PhysRevC.105.044319
10. W.R. Phillips, I. Ahmad, H. Emling et al., Octupole deformation in neutron-rich barium isotopes. Phys. Rev. Lett. **57**, 3257 (1986). https://doi.org/10.1103/PhysRevLett.57.3257
11. S.J. Zhu, Q.H. Lu, J.H. Hamilton et al., Octupole deformation in ^{142,143}Ba and ^{144}Ce: new band structures in neutron-rich Ba-isotopes. Phys. Lett. B **357**, 273–280 (1995). https://doi.org/10.1016/0370-2693(95)00900-6
12. W. Urban, M.A. Jones, J.L. Durell et al., Octupole correlations in neutron-rich, even-even barium isotopes. Nucl. Phys. A **613**, 107–131 (1997). https://doi.org/10.1016/S0375-9474(96)00393-4
13. S.J. Zhu, E.H. Wang, J.H. Hamilton et al., Coexistence of reflection asymmetric and symmetric shapes in ^{144}Ba. Phys. Rev. Lett. **124**, 032501 (2020). https://doi.org/10.1103/PhysRevLett.124.032501
14. B. Bucher, S. Zhu, C.Y. Wu et al., Direct evidence of octupole deformation in neutron-rich ^{144}Ba. Phys. Rev. Lett. **116**, 112503 (2016). https://doi.org/10.1103/PhysRevLett.116.112503
15. W. Nazarewicz, S.L. Tabor, Octupole shapes and shape changes at high spins in the Z≊58, N≊88 nuclei. Phys. Rev. C **45**, 2226 (1992). https://doi.org/10.1103/PhysRevC.45.2226
16. E. Garrote, J.L. Egido, L.M. Robledo, Fingerprints of reflection asymmetry at high angular momentum in atomic nuclei. Phys. Rev. Lett. **80**, 4398 (1998). https://doi.org/10.1103/PhysRevLett.80.4398
17. R.V. Jolos, P. von Brentano, Angular momentum dependence of the parity splitting in nuclei with octupole correlations. Phys. Rev. C **49**, 2301(R) (1994). https://doi.org/10.1103/PhysRevC.49.R2301
18. R.V. Jolos, P. von Brentano, Stabilization of octupole deformation with angular-momentum increase in the alternating-parity bands. Phys. Rev. C **92**, 044318 (2015). https://doi.org/10.1103/PhysRevC.92.044318
19. E.V. Mardyban, T.M. Shneidman, E.A. Kolganova et al., Analytical description of shape transition in nuclear alternating parity bands. Chin. Phys. C **42**, 124104 (2018). https://doi.org/10.1088/1674-1137/42/12/124104
20. N. Minkov, S.B. Drenska, P.P. Raychev et al., "Beat'' patterns for the odd-even staggering in octupole bands from a quadrupole-octupole Hamiltonian. Phys. Rev. C **63**, 044305 (2001). https://doi.org/10.1103/PhysRevC.63.044305
21. X. Zhang, Y. Peng, C.B. Zhou et al., Nuclear alternating parity bands and transition rates in a model of coherent quadrupole-octupole motion in neutron-rich barium isotopes. Nucl. Sci. Tech. **27**, 129 (2016). https://doi.org/10.1007/s41365-016-0128-0
22. T.M. Shneidman, G.G. Adamian, N.V. Antonenko et al., Cluster interpretation of properties of alternating parity bands in heavy nuclei. Phys. Rev. C **67**, 014313 (2003). https://doi.org/10.1103/PhysRevC.67.014313
23. T.M. Shneidman, G.G. Adamian, N.V. Antonenko et al., Description of alternating-parity bands within the dinuclear-system model. Phys. Atom. Nuclei **79**, 963–977 (2016). https://doi.org/10.1134/S1063778816060235
24. H.L. Wang, J. Yang, M.L. Liu et al., Evolution of ground-state quadrupole and octupole stiffnesses in even-even barium isotopes. Phys. Rev. C **92**, 024303 (2015). https://doi.org/10.1103/PhysRevC.92.024303
25. W. Zhang, Z.P. Li, S.Q. Zhang, Octupole deformation for Ba isotopes in a reflection-asymmetric relativistic mean-field approach. Chin. Phys. C **34**, 1094 (2010). https://doi.org/10.1088/1674-1137/34/8/011
26. W. Zhang, Y.F. Niu, Shape transition with temperature of the pear-shaped nuclei in covariant density functional theory. Phys. Rev. C **96**, 054308 (2017). https://doi.org/10.1103/PhysRevC.96.054308
27. W. Zhang, W. Cao, G.T. Zhang et al., OLevel density of odd-A nuclei at saddle point. Nucl. Sci. Tech. **34**, 124 (2023). https://doi.org/10.1007/s41365-023-01270-8

28. Y.C. Cao, S.E. Agbemava, A.V. Afanasjev et al., Landscape of pear-shaped even-even nuclei. Phys. Rev. C **102**, 024311 (2020). https://doi.org/10.1103/PhysRevC.102.024311
29. K. Nomura, D. Vretenar, T. Nikšić et al., Microscopic description of octupole shape-phase transitions in light actinide and rare-earth nuclei. Phys. Rev. C **89**, 024312 (2014). https://doi.org/10.1103/PhysRevC.89.024312
30. K. Nomura, R. Rodríguez-Guzmán, L.M. Robledo et al., Evolution of octupole deformation and collectivity in neutron-rich lanthanides. Phys. Rev. C **104**, 044324 (2021). https://doi.org/10.1103/PhysRevC.104.044324
31. R.N. Bernard, L.M. Robledo, T.R. Rodríguez, Octupole correlations in the ^{144}Ba nucleus described with symmetry-conserving configuration-mixing calculations. Phys. Rev. C **93**, 061302 (2016). https://doi.org/10.1103/PhysRevC.93.061302
32. J.M. Yao, E.F. Zhou, Z.P. Li, Beyond relativistic mean-field approach for nuclear octupole excitations. Phys. Rev. C **92**, 041304 (2015). https://doi.org/10.1103/PhysRevC.92.041304
33. Y. Fu, H. Wang, L.-J. Wang et al., Odd-even parity splittings and octupole correlations in neutron-rich Ba isotopes. Phys. Rev. C **97**, 024338 (2018). https://doi.org/10.1103/PhysRevC.97.024338
34. Relativistic Density Functional for Nuclear Structure, in International Review of Nuclear Physics, ed. by J. Meng, (World Scientific, Singapore, 2016), Vol. 10
35. M. Bender, P.H. Heenen, Self-consistent mean-field models for nuclear structure. Rev. Mod. Phys. **75**, 121 (2003). https://doi.org/10.1103/RevModPhys.75.121
36. W. Zhang, Z.P. Li, Zhang, et al., used Octupole degrees of freedom for the critical-point candidate nucleus ^{152}Sm in a reflection-asymmetric relativistic mean-field approach. Phys. Rev. C **81**, 034302 (2010). https://doi.org/10.1103/PhysRevC.81.034302
37. S.Y. Wang, Z.L. Zhu, Z.M. Niu, Influence of the Coulomb exchange term on nuclear single-proton resonances. Nucl. Sci. Tech. **27**, 122 (2016). https://doi.org/10.1007/s41365-016-0125-3
38. S.Y. Xia, H. Tao, Y. Lu et al., Spectroscopy of reflection-asymmetric nuclei with relativistic energy density functionals. Phys. Rev. C **96**, 054303 (2017). https://doi.org/10.1103/PhysRevC.96.054303
39. W. Sun, S. Quan, Z.P. Li et al., Microscopic core-quasiparticle coupling model for spectroscopy of odd-mass nuclei with octupole correlations. Phys. Rev. C **100**, 044319 (2019). https://doi.org/10.1103/PhysRevC.100.044319
40. Y.T. Wang, T.T. Sun, Searching for single-particle resonances with the Green's function method. Nucl. Sci. Tech. **32**, 46 (2021). https://doi.org/10.1007/s41365-021-00884-0
41. T.H. Heng, Y.W. Chu, Properties of Titanium isotopes in complex momentum representation within relativistic mean-field theory. Nucl. Sci. Tech. **33**, 117 (2022). https://doi.org/10.1007/s41365-022-01098-8
42. E.B. Huo, K.R. Li, X.Y. Qu et al., Continuum Skyrme Hartree-Fock-Bogoliubov theory with Green's function method for neutron-rich Ca, Ni, Zr, and Sn isotopes. Nucl. Sci. Tech. **34**, 105 (2023). https://doi.org/10.1007/s41365-023-01261-9
43. R. An, S. Sun, L.G. Cao et al., Constraining nuclear symmetry energy with the charge radii of mirror-pair nuclei. Nucl. Sci. Tech. **34**, 119 (2023). https://doi.org/10.1007/s41365-023-01269-1
44. K.P. Geng, P.X. Du, D.L. Fang, Calculation of microscopic nuclear level densities based on covariant density functional theory. Nucl. Sci. Tech. **34**, 141 (2023). https://doi.org/10.1007/s41365-022-01140-9
45. X.X. Sun, S.G. Zhou, Deformed halo nuclei and shape decoupling effects. Nuclear Techniques **46**, 080015 (2023). https://doi.org/10.11889/j.0253-3219.2023.hjs.46.080015 (in Chinese)
46. L. Guo, Y.F. Niu, Effects of isoscalar pairing force on spin-isospin transitions in ^{42}Ca. Nuclear Techniques **46**, 080019 (2023). https://doi.org/10.11889/j.0253-3219.2023.hjs.46.080019 (in Chinese)
47. J. Peng, J. Meng, P. Ring et al., Covariant density functional theory for magnetic rotation. Phys. Rev. C **78**, 024313 (2008). https://doi.org/10.1103/PhysRevC.78.024313
48. P.W. Zhao, S.Q. Zhang, J. Peng et al., Novel structure for magnetic rotation bands in ^{60}Ni. Phys. Lett. B **699**, 181–186 (2011). https://doi.org/10.1016/j.physletb.2011.03.068
49. P.W. Zhao, J. Peng, H.Z. Liang et al., Antimagnetic rotation band in nuclei: a microscopic description. Phys. Rev. Lett. **107**, 122501 (2011). https://doi.org/10.1103/PhysRevLett.107.122501
50. P.W. Zhao, Multiple chirality in nuclear rotation: A microscopic view. Phys. Lett. B **773**, 1–5 (2017). https://doi.org/10.1016/j.physletb.2017.08.001
51. Z.X. Ren, S.Q. Zhang, P.W. Zhao et al., Stability of the linear chain structure for ^{12}C in covariant density functional theory on a 3D lattice. Sci. China Phys. Mech. Astron. **62**, 112062 (2019). https://doi.org/10.1007/s11433-019-9412-3
52. D.D. Zhang, Z.X. Ren, P.W. Zhao et al., Effects of rotation and valence nucleons in molecular α-chain nuclei. Phys. Rev. C **105**, 024322 (2022). https://doi.org/10.1103/PhysRevC.105.024322
53. Z.X. Ren, P.W. Zhao, S.Q. Zhang et al., Toroidal states in 28Si with covariant density functional theory in 3D lattice space. Nucl. Phys. A **996**, 121696 (2020). https://doi.org/10.1016/j.nuclphysa.2020.121696
54. Z.X. Ren, P.W. Zhao, J. Meng, Dynamics of rotation in chiral nuclei. Phys. Rev. C **105**, L011301 (2022). https://doi.org/10.1103/PhysRevC.105.L011301
55. P. Ring, Relativistic mean field theory in finite nuclei. Prog. Part. Nucl. Phys. **37**, 193–263 (1996). https://doi.org/10.1016/0146-6410(96)00054-3
56. D. Vretenar, A.V. Afanasjev, G.A. Lalazissis et al., Relativistic Hartree-Bogoliubov theory: static and dynamic aspects of exotic nuclear structure. Phys. Rep. **409**, 101–259 (2005). https://doi.org/10.1016/j.physrep.2004.10.001
57. J. Meng, H. Toki, S.G. Zhou et al., Relativistic continuum Hartree Bogoliubov theory for ground-state properties of exotic nuclei. Prog. Part. Nucl. Phys. **57**, 470–563 (2006). https://doi.org/10.1016/j.ppnp.2005.06.001
58. B.A. Nikolaus, T. Hoch, D.G. Madland, Nuclear ground state properties in a relativistic point coupling model. Phys. Rev. C **46**, 1757 (1992). https://doi.org/10.1103/PhysRevC.46.1757
59. T. Bürvenich, D.G. Madland, J.A. Maruhn et al., Nuclear ground state observables and QCD scaling in a refined relativistic point coupling model. Phys. Rev. C **65**, 044308 (2002). https://doi.org/10.1103/PhysRevC.65.044308
60. P.W. Zhao, Z.P. Li, J.M. Yao et al., New parametrization for the nuclear covariant energy density functional with a point-coupling interaction. Phys. Rev. C **82**, 054319 (2010). https://doi.org/10.1103/PhysRevC.82.054319
61. S. Frauendorf, J. Meng, Tilted rotation of triaxial nuclei. Nucl. Phys. A **617**, 131–147 (1997). https://doi.org/10.1016/S0375-9474(97)00004-3
62. J. Meng, J. Peng, S.Q. Zhang et al., Progress on tilted axis cranking covariant density functional theory for nuclear magnetic and antimagnetic rotation. Front. Phys. **8**, 55–79 (2013). https://doi.org/10.1007/s11467-013-0287-y
63. S. Frauendorf, Spontaneous symmetry breaking in rotating nuclei. Rev. Mod. Phys. **73**, 463–514 (2001). https://doi.org/10.1103/RevModPhys.73.463
64. S.G. Zhou, Multidimensionally constrained covariant density functional theories-nuclear shapes and potential energy surfaces. Phys. Scr. **91**, 063008 (2016). https://doi.org/10.1088/0031-8949/91/6/063008
65. Y.P. Wang, J. Meng, Nuclear chiral rotation induced by superfluidity. Phys. Lett. B **841**, 137923 (2023). https://doi.org/10.1016/j.physletb.2023.137923

66. G.A. Leander, Y.S. Chen, Reflection-asymmetric rotor model of odd A~219-229 nuclei. Phys. Rev. C **37**, 2744 (1988). https://doi.org/10.1103/PhysRevC.37.2744
67. F.F. Xu, Y.P. Wang, Shell-model-like approach based on covariant density functional theory in 3D lattice space: Evolution of octupole shape in rotating ^{224}Th. Int. J. Mod. Phys. E **32**, 2340007 (2023). https://doi.org/10.1142/S0218301323400074